Biexcitons are bound in $CsPbBr_3$ perovskite nanocrystals

Yoonjae Park [1,2] and David T. Limmer [1,2,3,4,*]

[1] *Department of Chemistry, University of California, Berkeley, California 94720, USA*
[2] *Materials Science Division, Lawrence Berkeley National Laboratory, Berkeley, California 94720, USA*
[3] *Chemical Science Division, Lawrence Berkeley National Laboratory, Berkeley, California 94720, USA*
[4] *Kavli Energy NanoScience Institute, Berkeley, California 94720, USA*

(Received 24 July 2023; accepted 12 October 2023; published 25 October 2023)

We study the energetics of quasiparticle excitations in $CsPbBr_3$ perovskite nanocrystals using path integral molecular dynamics simulations. Employing detailed molecular models, we elucidate the interplay of anharmonic lattice degrees of freedom, dielectric confinement, and electronic correlation on exciton and biexciton binding energies of a range of nanocrystal sizes. We find generally good agreement with some experimental observations of binding energies and additionally explain the observed size-dependent Stokes shift. The explicit model calculations are compared with simplified approximations to rationalize the lattice contributions to binding. We find that polaron formation significantly reduces exciton binding energies, whereas these effects are negligible for biexciton interactions. While experimentally the binding energy of biexcitons is uncertain, based on our study, we conclude that biexcitons are bound in $CsPbBr_3$.

DOI: 10.1103/PhysRevMaterials.7.106002

I. INTRODUCTION

Lead halide perovskite nanocrystals are currently the subject of significant interest due to their exceptionally high photoluminescence quantum yields, which make them ideal materials for light emission, lasing, and photodetection [1–5]. The electronic properties of the lead halides depend strongly on the coupling between charges and their surrounding soft, polar lattices [6–11]. This coupling has been implicated in several phenomena including photoinduced phase transitions, long radiative recombination rates, and anomalous temperature-dependent mobilities [12–16]. In nanocrystals, optical properties are largely determined by the behavior of exciton complexes [17]. Recently, Dana *et al.* [18] proposed a potential antibinding of biexcitons in perovskite nanocrystals, implicating the potential role of the lattice in mediating this interaction. Here, we study the energetics of quasiparticle excitations including excitons and biexcitons with an explicit description of the lattice, over a range of perovskite nanocrystal sizes. We find that, while polaron formation weakens the exciton binding energy, biexciton energetics are largely unaffected, leading to an expectation that they are bound in nanocrystals and in bulk.

Excitons and biexcitons are both characterized by a binding energy, the energy required to dissociate the pair of quasiparticles—free charges or excitons. While there is reasonable consensus on the bulk exciton binding energy [19–24], its dependence on nanocrystal size is less certain. Further, a number of biexciton binding energies have been reported experimentally for lead halide perovskites, but their values span a large range and even disagree in sign [2,3,18,25–31]. Experimental measurements are hampered by the nanocrystal polydispersity, spectral drift, and thermal broadening of spectral lines [32–34]. These ambiguities could be clarified theoretically; however, there are few suitable approaches available. Unlike traditional semiconductors where structural fluctuations can be ignored or described within a harmonic approximation, the perovskite lattice structure with its anharmonic tilting and rocking motions results in significant renormalization of electronic properties [35–37]. Given that incorporating the effects from the lattice is important in understanding excitonic properties, there have been some attempts to include them in a theoretical description. For example, extensions to GW and Bethe-Salpeter equations have been developed to include phonon effects on excitonic properties perturbatively [38–44]. At the same time, quasiparticle excitations require a balanced description of electron correlation, making *ab initio* models difficult to apply in nanocrystals where the number of atoms is large. Tight-binding and pseudopotential models have been developed to study excitonic structure, but these have not yet been unified with approaches to describe electron-phonon effects [45–48].

II. THEORETICAL MODEL OF $CsPbBr_3$ NANOCUBES

We use quasiparticle path integral molecular dynamics [49] with an explicit atomistic description of the lattice, which allows us to include all orders of anharmonicity from the lattice and treat electron correlation exactly. This approach has been previously successful at describing the excitonic properties of bulk systems [15,37], and the lattice model we employ has been used extensively to describe both vibrational and nonlinear properties of a variety of lead halide systems [48,50–52]. In this paper, we consider a system of

*dlimmer@berkeley.edu

a single biexciton interacting with $CsPbBr_3$ cubic perovskite nanocrystals. The model Hamiltonian consists of three pieces: $\mathcal{H} = \mathcal{H}_{\rm el} + \mathcal{H}_{\rm lat} + \mathcal{H}_{\rm int}$. Within an effective mass approximation, valid because of the highly dispersive bands [53], the electronic Hamiltonian $\mathcal{H}_{\rm el}$ is defined by kinetic energies and Coulomb interactions between electrons and holes:

$$\mathcal{H}_{\rm el} = \sum_i \frac{\hat{\mathbf{p}}_i^2}{2m_i} + \sum_{i\neq j} \frac{q_i q_j}{4\pi\varepsilon_\infty |\hat{\mathbf{x}}_i - \hat{\mathbf{x}}_j|}, \tag{1}$$

where the subscripts $i, j \in \{e_1, e_2, h_1, h_2\}$ indicate two electrons and two holes, respectively, $\hat{\mathbf{p}}$ and $\hat{\mathbf{x}}$ are momentum and position operators, m_i is the band mass set to 0.22 m_0 and 0.24 m_0 for electrons and holes in terms of the bare electron mass m_0, $\varepsilon_\infty = 4.3$ is the optical dielectric constant in the unit of vacuum permittivity ε_0, and q is the charge of the quantum particle which is $-e$ for electrons and $+e$ for holes [54]. We consider a singlet biexciton, so electrons and holes are distinguishable particles [55].

For the lattice, we model the $CsPbBr_3$ nanocrystals explicitly using a previously validated *ab initio* derived force field [48,50]. Its Hamiltonian is given by

$$\mathcal{H}_{\rm lat} = \sum_{i=1}^{N} \frac{\mathbf{p}_i^2}{2m_i} + U_{\rm lat}(\mathbf{x}_{\rm lat}), \tag{2}$$

where $\mathbf{x}_{\rm lat} = \{\mathbf{x}_1, \mathbf{x}_2, \ldots, \mathbf{x}_N\}$ are the positions of the N atoms in the lattice, $\mathbf{p}_i$ and m_i are the momentum and mass for the ith atom. The atomistic force field $U_{\rm lat}$ is the sum of pairwise interactions with distance $x_{ij} = |\mathbf{x}_i - \mathbf{x}_j|$ consisting of a Coulomb potential and Lennard-Jones potential [50]:

$$U_{\rm lat} = \sum_{i,j=1}^{N} \frac{q_i q_j}{4\pi\varepsilon_0 x_{ij}} + 4\varepsilon_{ij}\left[\left(\frac{\sigma_{ij}}{x_{ij}}\right)^{12} - \left(\frac{\sigma_{ij}}{x_{ij}}\right)^{6}\right], \tag{3}$$

where the parameters q_i, ε_{ij}, and σ_{ij} are summarized in Table S1 in the Supplemental Material [56]. The interaction between the quasiparticles and lattice is written as the sum of pseudopotentials between each quantum particle i and the lattice particle j:

$$\mathcal{H}_{\rm int} = \sum_i \sum_{j=1}^{N} \frac{q_i q_j}{4\pi\varepsilon_0 \sqrt{r_{\rm cut}^2 + |\hat{\mathbf{x}}_i - \hat{\mathbf{x}}_j|^2}}, \tag{4}$$

where the cutoff distances $r_{\rm cut}$ are chosen using the atomic radii of each atom [15,49,57,58].

The quasiparticle interactions are screened by the optical dielectric constant of the nanocrystal, which changes discontinuously at the boundary between the perovskite and surrounding solution. To account for the dielectric discontinuity, we use a multipole expansion [59], resulting in an effective potential for each charge:

$$U_{\rm wall} = \sum_{i,k} \frac{q_i^2}{8\pi\varepsilon_0 |\hat{\mathbf{x}}_i - \mathbf{x}_{{\rm wall},k}|} \cdot \frac{\varepsilon_\infty - \varepsilon_0}{\varepsilon_\infty + \varepsilon_0}, \tag{5}$$

where $i \in \{e_1, e_2, h_1, h_2\}$, $k \in \{\pm x, \pm y, \pm z\}$, and $\mathbf{x}_{{\rm wall},k} = \pm L/2$ is the position of the wall, with L as the edge length of the nanocrystal. This external potential results in a dielectric confinement. Additional details on the atomistic force field, pseudopotentials, and wall potentials are described in the Supplemental Material [56].

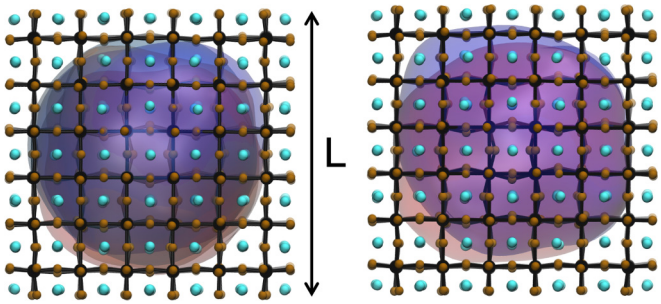

FIG. 1. Simulation snapshot of biexciton (left) and exciton (right) interacting with $CsPbBr_3$ perovskite nanocrystal, where $L = 3.56$ nm represents the edge length of the nanocrystal.

For electrons and holes, we use imaginary time path integrals [60,61], while the heavy atoms of the lattice are treated classically. The resultant partition function $\mathcal{Z}$ can be written as

$$\mathcal{Z} = \int \mathcal{D}[\mathbf{x}_{eh}(\tau),\, \mathbf{x}_{\rm lat}] \exp\left\{-\int_{\tau=0}^{\beta\hbar} \frac{\mathcal{H}[\mathbf{x}_{eh}(\tau),\, \mathbf{x}_{\rm lat}]}{\hbar}\right\}, \tag{6}$$

where $\mathbf{x}_{eh}(\tau) = \{\mathbf{x}_{e_1}(\tau), \mathbf{x}_{e_2}(\tau), \mathbf{x}_{h_1}(\tau), \mathbf{x}_{h_2}(\tau)\}$, where $\mathbf{x}_i(\tau)$ is the position of quantum particle i at imaginary time τ, $\hbar$ is the Planck's constant, and $\beta^{-1} = k_{\rm B}T$, with $k_{\rm B}$ and T as the Boltzmann constant and temperature. Discretizing the path action renders each quantum particle isomorphic to a ring polymer, where neighboring time slices are connected by harmonic springs [55,62]. We use molecular dynamics simulations with a second-order discretization of the path integral to compute expectation values of this system, for which each quantum particle is represented by 1000 time slices. Representative simulation snapshots of both the biexciton and exciton are shown in Fig. 1. Throughout, we consider nanocrystalline cubes, where L is the edge length.

For comparison, we also consider two approximate models that incorporate harmonic and static lattice effects. To incorporate effects from harmonic phonons, we adopt a dynamic screening model described previously [15,37], which is a model for charges that are coupled linearly with the polarization field generated by a collection of harmonic modes. In this model, lattice variables are analytically integrated out, resulting in an imaginary time influence functional that can be studied straightforwardly numerically. We parametrize the influence functional with a Frohlich coupling for the electrons and holes $\alpha_e = 2.65$ and $\alpha_h = 2.76$ and an optical phonon mode with energy $\hbar\omega = 16.8$ meV [54]. We also compare a static lattice, where only the electronic Hamiltonian and confinement effects are considered. All simulations are done in LAMMPS [63], and the details of the discretized Hamiltonian can be found in the Supplemental Material [56].

III. QUASIPARTICLE BINDING ENERGIES

With an explicit lattice, the exciton binding energy is

$$\Delta_X = \lim_{T\to 0} \langle E\rangle_{\rm e} + \langle E\rangle_{\rm h} - \langle E\rangle_{\rm ex} - \langle U_{\rm lat}\rangle_{\rm ex},$$

while the biexciton binding energy is

$$\Delta_{XX} = \lim_{T\to 0} 2\langle E\rangle_{\rm ex} - \langle E\rangle_{\rm biex} - \langle U_{\rm lat}\rangle_{\rm ex},$$

where the subscripts biex and ex refer to simulations of a biexciton (two electrons and two holes) and exciton (electron and hole), while e/h indicates a simulation with only electron/hole interacting with the surrounding lattice. Simulations are performed at 50 K, which is low enough to extract the ground-state energy. The binding energies are computed from the average energy [64]:

$$\langle E\rangle = -\frac{\partial}{\partial\beta}\ln \mathcal{Z}[\mathbf{x}_{eh}(\tau), \mathbf{x}_{\rm lat}(\tau)], \tag{7}$$

where $\mathbf{x}_{eh} = \{\mathbf{x}_{e_1}, \mathbf{x}_{h_1}\}$ or $\mathbf{x}_{eh} = \{\mathbf{x}_{e_1}, \mathbf{x}_{e_2}, \mathbf{x}_{h_1}, \mathbf{x}_{h_2}\}$ for an exciton and biexciton, respectively. The derivative above produces two terms, an average kinetic energy and an average potential energy, where we use a virial estimator [65] to efficiently estimate the kinetic energy. For the evaluation of binding energies from the simulations with only quasiparticles, in the static or dynamic approximation, the same definitions are used without the lattice relevant terms. Within the static approximation, the binding energies are determined by only $\mathcal{H}_e$ and the confining potential. To efficiently extract the binding energies with dynamic approximation, we use a thermodynamic perturbative theory approach [56].

Figure 2(a) shows the exciton binding energy Δ_X computed from our molecular model in addition to those approximated with the static or dynamic models for the nanocubes considered, ranging from $L = 2.4$ to 6 nm. Given the reduced mass of the exciton $\mu = 0.11$ and optical dielectric constant, the Bohr radius of the exciton is $R_X = 2.07$ nm. Thus, for the range of nanocrystals considered, we are in a moderate to strong confinement regime. As a consequence, all binding energy estimates exhibit a strong L dependence, which we model in Fig. 2(a) as $\Delta_X = \Delta_X^\circ(1 + \ell_1/L + \ell_2^2/L^2)$, where Δ_X° is the bulk binding energy, and ℓ_1 and ℓ_2 are fit parameters, taken here as purely phenomenological but which can be deduced from perturbation theory [67,68].

Over the full range of nanocrystal sizes considered, the static approximation yields a binding energy much larger than either the explicit model calculation or the dynamic approximation. The value from the static approximation with the largest nanocrystal reasonably agrees with the expectation from a Wannier-Mott model $\Delta_{X,\rm WM} = R_H\mu/\varepsilon_\infty^2 = 84.5$ meV, where R_H is a Rydberg energy. The values at finite L agree well with recent pseudopotential-based calculations of $CsPbI_3$, up to a shift of the bulk binding energy by 20 meV to account for the change in halide [48].

The explicit model calculations are reproduced well by the dynamic approximation. The suppression of the binding energy due to lattice effects could arise because of two distinct mechanisms. First, the lattice could screen the electron-hole interactions, weakening them. Second, the lattice can lower the self-energies of the free charges, bringing them closer to the exciton self-energy, effectively reducing the binding energy. In agreement with previous calculations on bulk $MAPbI_3$ [37], we find the latter effect is more prominent. This effect is outside of first-order perturbation theory that overestimates the decrease in the self-energy of the free charges, which we find is −30 meV for both charges, and ignores the decrease in self-energy of the polaron-exciton, which is −12 meV. With the explicit perovskite lattice, the extrapolated value to the large nanocrystal size limit is in good agreement with bulk $CsPbBr_3$ exciton binding energy of 40 meV, reflecting slight anharmonic weakening of the optical phonon [19–24].

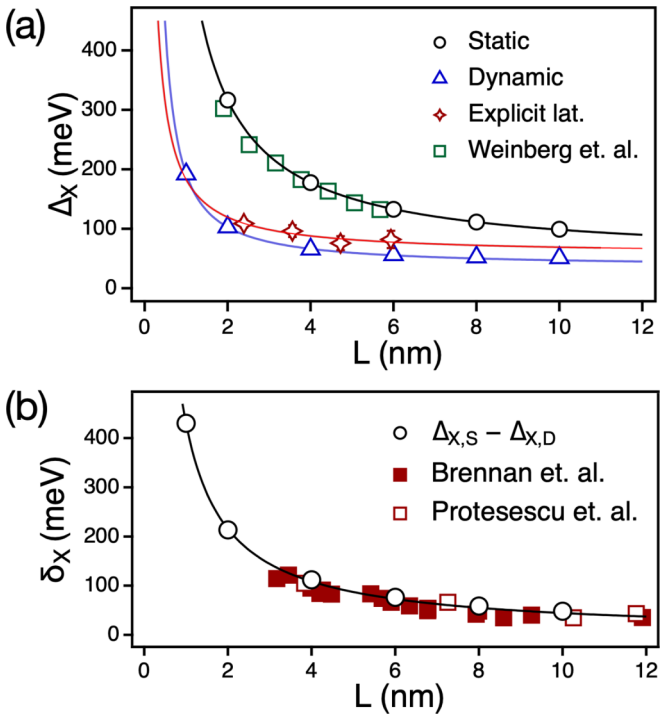

FIG. 2. Energetics of exciton formation. (a) Exciton binding energy under static ($\Delta_{X,S}$ black circles), dynamic ($\Delta_{X,D}$ blue triangles), and explicit lattice (red stars) models. Comparison to Weinberg *et al.* [48] is shown in green squares. (b) The difference in the exciton binding energies from dynamic and static screenings, which is defined as $\delta_X = \Delta_{X,S} - \Delta_{X,D}$ compared with Stokes shift measurements from Brennan *et al.* [66] and Protesescu *et al.* [19]. Solid lines are fits to $\Delta_X = \Delta_X^\circ(1 + \ell_1/L + \ell_2^2/L^2)$ and $\delta_X = \delta_X^\circ(1 + \ell'/L)$, with $\ell_1 =$ 10.5, 3.2, and 2.2 nm, $\ell_2 = 1.2, 1.1,$ and 0 nm for static, dynamic, explicit lattices, respectively, and $\ell' = 257$ nm.

Shown in Fig. 2(b) is the difference between the dynamic and static screening models $\delta_X = \Delta_{X,S} - \Delta_{X,D}$. This energy is due to polaron formation. The strong nanocrystal size dependence reflects the increasing confinement of the charges, which lower their self-energy by increasing their localization, as the energy of a charge in a dielectric will decrease like $1/L$, which fits δ_X well. We find the polaron formation energy agrees well with size-dependent Stokes shift measurements made from the difference between absorption and emission spectra [69]. Results from two different experiments on $CsPbBr_3$ nanocrystals [19,70] compare quantitatively well with our computed δ_X, increasing from 10 meV to >450 meV. Previously, a lattice origin of the Stokes shift had been disregarded due to the relatively small polaron formation energy in the bulk [70]. However, we find the polaron formation energy can increase substantially in small nanocrystals.

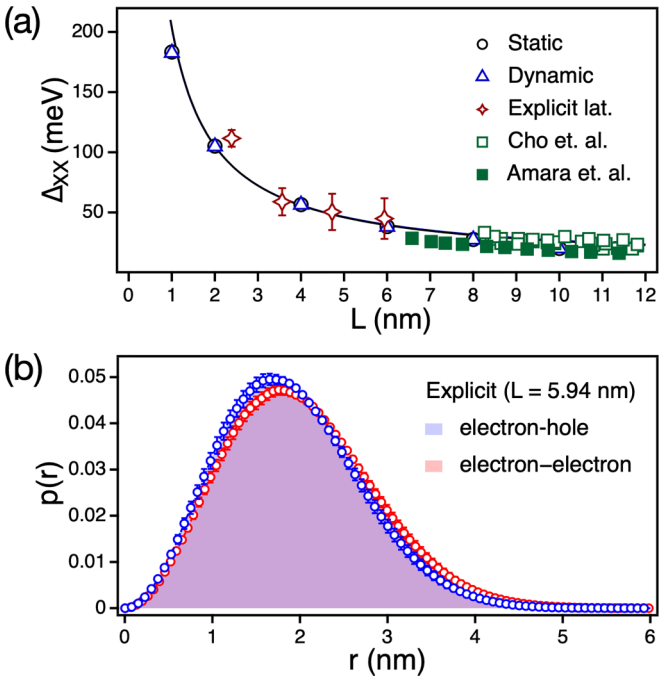

FIG. 3. Energetics and structure of biexcitons. (a) Biexciton binding energies for our explicit model (red stars) and its dynamical (blue triangles) and static (black circles) approximations. Comparisons with Cho *et al.* [28] and Amara *et al.* [26] are shown in green squares. The solid line is a fit to $\Delta_{XX} = \Delta^{\circ}_{XX}(1 + \tilde{\ell}_1/L + \tilde{\ell}_2{}^2/L^2)$, with $\tilde{\ell}_1 = 30.4$ nm and $\tilde{\ell}_2 \approx 0$ nm. (b) Electron-hole (blue) and electron-electron (red) distributions of biexciton from the simulations with explicit lattice.

With the excitonic energetics understood, we now turn to the binding of biexcitons. The biexciton binding energy Δ_{XX} for the explicit model as well as the static and dynamic approximations are shown in Fig. 3(a). All three models agree quantitatively, indicating that contrary to expectations from the exciton calculations, lattice effects are unimportant for biexciton binding. We rationalize this by noting that the primary contribution from the lattice for the exciton was the stabilization of the free charges due to the polaron formation, which does not contribute to the biexciton energy.

In Fig. 3(b) are the electron-hole and electron-electron radial probability distributions $p(r)$ from simulations with the explicit lattice, where electron-electron repulsion makes the average distance slightly larger than the average electron-hole distance. However, this increase is small, and their size is largely determined by confinement rather than electron correlation. Similar masses for the electron and hole produce a very weak dipole in the exciton or quadrapole in the biexciton that is not large enough to generate a polarization response from the lattice. Further, the similar results in both binding energies from the explicit lattice and dynamic models imply that the anharmonicity coming from the explicit perovskite lattice does not play a crucial role in determining the behavior of biexcitons, likely due to the relatively small amplitude distortion. However, Δ_{XX} is relatively large, between a half and a quarter of Δ_X, indicating the importance of electron correlation.

As with Δ_X, we find a strong system size dependence of Δ_{XX}, increasing strongly with decreasing L. We model this dependence as $\Delta_{XX} = \Delta^{\circ}_{XX}(1 + \tilde{\ell}_1/L + \tilde{\ell}_2{}^2/L^2)$, with $\tilde{\ell}_1$ and $\tilde{\ell}_2$ employed as fitting parameters. While experimentally values of Δ_{XX} have been reported between -100 and 100 meV [2,3,18,25–31], recent size-dependent measurements on $CsPbBr_3$ nanocubes from two different groups [26,28] are shown in Fig. 3(a) and agree well with our results. To our knowledge, these data are the only systematic size-dependent binding energies available experimentally.

IV. CONCLUSION

In summary, we employed path-integral molecular dynamics simulations to study quasiparticle energetics in perovskite nanocrystals. Using atomic models and simple approximations, we can systematically explore the roles of the lattice effects on exciton and biexciton binding energies. We found that the lattice renormalizes the exciton binding energy significantly in nanocrystals but not biexciton binding energies, likely due to the weak coupling between the la ttice and the neutral exciton complex. We found that biexcitons are bound regardless of the size and the type of screening employed, which strongly suggests that experimental reports of antibinding in $CsPbBr_3$ are misinterpreted. We hope that the quantification of the energies reported here can help better constrain fitting of transient absorption data.

ACKNOWLEDGMENTS

This work was supported by the US Department of Energy, Office of Science, Office of Basic Energy Sciences, Materials Sciences and Engineering Division, under Contract No. DE-AC02-05CH11231 within the Fundamentals of Semiconductor Nanowire Program (KCPY23). Y.P. acknowledges the Kwanjeong Educational Foundation. D.T.L. acknowledges the Alfred P. Sloan Foundation.

[1] K. Hong, Q. V. Le, S. Y. Kim, and H. W. Jang, J. Mater. Chem. C **6**, 2189 (2018).
[2] G. Yumoto and Y. Kanemitsu, Phys. Chem. Chem. Phys. **24**, 22405 (2022).
[3] C. Zhu, T. Nguyen, S. C. Boehme, A. Moskalenko, D. N. Dirin, M. I. Bodnarchuk, C. Katan, J. Even, G. Rainó, and M. V. Kovalenko, Adv. Mater. **35**, 2208354 (2023).
[4] R. Ahumada-Lazo, R. Saran, O. Woolland, Y. Jia, M.-E. Kyriazi, A. G. Kanaras, D. Binks, and R. J. Curry, J. Phys.: Photonics **3**, 021002 (2021).
[5] B. R. C. Vale, E. Socie, A. Burgos-Caminal, J. Bettini, M. A. Schiavon, and J.-E. Moser, J. Phys. Chem. Lett. **11**, 387 (2020).
[6] P. P. Joshi, S. F. Maehrlein, and X. Zhu, Adv. Mater. **31**, 1803054 (2019).

[7] D. A. Egger, A. Bera, D. Cahen, G. Hodes, T. Kirchartz, L. Kronik, R. Lovrincic, A. M. Rappe, D. R. Reichman, and O. Yaffe, Adv. Mater. **30**, 1800691 (2018).

[8] D. T. Limmer and N. S. Ginsberg, J. Chem. Phys. **152**, 230901 (2020).

[9] D. A. Egger, A. M. Rappe, and L. Kronik, Acc. Chem. Res. **49**, 573 (2016).

[10] J. Berry, T. Buonassisi, D. A. Egger, G. Hodes, L. Kronik, Y.-L. Loo, I. Lubomirsky, S. R. Marder, Y. Mastai, J. S. Miller *et al.*, Adv. Mater. **27**, 5102 (2015).

[11] M. J. Schilcher, P. J. Robinson, D. J. Abramovitch, L. Z. Tan, A. M. Rappe, D. R. Reichman, and D. A. Egger, ACS Energy Lett. **6**, 2162 (2021).

[12] C. G. Bischak, C. L. Hetherington, H. Wu, S. Aloni, D. F. Ogletree, D. T. Limmer, and N. S. Ginsberg, Nano Lett. **17**, 1028 (2017).

[13] M. Z. Mayers, L. Z. Tan, D. A. Egger, A. M. Rappe, and D. R. Reichman, Nano Lett. **18**, 8041 (2018).

[14] S. D. Stranks, G. E. Eperon, G. Grancini, C. Menelaou, M. J. Alcocer, T. Leijtens, L. M. Herz, A. Petrozza, and H. J. Snaith, Science **342**, 341 (2013).

[15] Y. Park, A. Obliger, and D. T. Limmer, Nano Lett. **22**, 2398 (2022).

[16] B. A. A. Martin and J. M. Frost, Phys. Rev. B **107**, 115203 (2023).

[17] W. Zhao, Z. Qin, C. Zhang, G. Wang, X. Huang, B. Li, X. Dai, and M. Xiao, J. Phys. Chem. Lett. **10**, 1251 (2019).

[18] J. Dana, T. Binyamin, L. Etgar, and S. Ruhman, ACS Nano **15**, 9039 (2021).

[19] L. Protesescu, S. Yakunin, M. I. Bodnarchuk, F. Krieg, R. Caputo, C. H. Hendon, R. X. Yang, A. Walsh, and M. V. Kovalenko, Nano Lett. **15**, 3692 (2015).

[20] S. Parveen, K. K. Paul, R. Das, and P. Giri, J. Colloid Interface Sci. **539**, 619 (2019).

[21] R. X. Yang and L. Z. Tan, J. Chem. Phys. **152**, 034702 (2020).

[22] J. Li, L. Luo, H. Huang, C. Ma, Z. Ye, J. Zeng, and H. He, J. Phys. Chem. Lett. **8**, 1161 (2017).

[23] K. Zheng, Q. Zhu, M. Abdellah, M. E. Messing, W. Zhang, A. Generalov, Y. Niu, L. Ribaud, S. E. Canton, and T. Pullerits, J. Phys. Chem. Lett. **6**, 2969 (2015).

[24] S. M. H. Qaid, H. M. Ghaithan, B. A. Al-Asbahi, and A. S. Aldwayyan, ACS Omega **6**, 5297 (2021).

[25] M. N. Ashner, K. E. Shulenberger, F. Krieg, E. R. Powers, M. V. Kovalenko, M. G. Bawendi, and W. A. Tisdale, ACS Energy Lett. **4**, 2639 (2019).

[26] M.-R. Amara, Z. Said, C. Huo, A. Pierret, C. Voisin, W. Gao, Q. Xiong, and C. Diederichs, Nano Lett. **23**, 3607 (2023).

[27] N. S. Makarov, S. Guo, O. Isaienko, W. Liu, I. Robel, and V. I. Klimov, Nano Lett. **16**, 2349 (2016).

[28] K. Cho, T. Yamada, H. Tahara, T. Tadano, H. Suzuura, M. Saruyama, R. Sato, T. Teranishi, and Y. Kanemitsu, Nano Lett. **21**, 7206 (2021).

[29] G. Yumoto, H. Tahara, T. Kawawaki, M. Saruyama, R. Sato, T. Teranishi, and Y. Kanemitsu, J. Phys. Chem. Lett. **9**, 2222 (2018).

[30] J. Aneesh, A. Swarnkar, V. K. Ravi, R. Sharma, A. Nag, and K. V. Adarsh, J. Phys. Chem. C **121**, 4734 (2017).

[31] J. A. Castaneda, G. Nagamine, E. Yassitepe, L. G. Bonato, O. Voznyy, S. Hoogland, A. F. Nogueira, E. H. Sargent, C. H. B. Cruz, and L. A. Padilha, ACS Nano **10**, 8603 (2016).

[32] G. Lubin, R. Tenne, A. C. Ulku, I. M. Antolovic, S. Burri, S. Karg, V. J. Yallapragada, C. Bruschini, E. Charbon, and D. Oron, Nano Lett. **21**, 6756 (2021).

[33] F. V. Antolinez, F. T. Rabouw, A. A. Rossinelli, J. Cui, and D. J. Norris, Nano Lett. **19**, 8495 (2019).

[34] A. P. Beyler, L. F. Marshall, J. Cui, X. Brokmann, and M. G. Bawendi, Phys. Rev. Lett. **111**, 177401 (2013).

[35] J. Pollmann and H. Büttner, Phys. Rev. B **16**, 4480 (1977).

[36] H. Haken, Z. Physik **146**, 527 (1956).

[37] Y. Park and D. T. Limmer, J. Chem. Phys. **157**, 104116 (2022).

[38] M. R. Filip, J. B. Haber, and J. B. Neaton, Phys. Rev. Lett. **127**, 067401 (2021).

[39] M. Schlipf, S. Poncé, and F. Giustino, Phys. Rev. Lett. **121**, 086402 (2018).

[40] W. H. Sio, C. Verdi, S. Poncé, and F. Giustino, Phys. Rev. B **99**, 235139 (2019).

[41] W. H. Sio and F. Giustino, Nat. Phys. **19**, 629 (2023).

[42] M. Rohlfing and S. G. Louie, Phys. Rev. B **62**, 4927 (2000).

[43] S. Albrecht, L. Reining, R. Del Sole, and G. Onida, Phys. Stat. Sol. (a) **170**, 189 (1998).

[44] L. Hedin, Phys. Rev. **139**, A796 (1965).

[45] Y. Cho and T. C. Berkelbach, J. Phys. Chem. Lett. **10**, 6189 (2019).

[46] G. Biffi, Y. Cho, R. Krahne, and T. C. Berkelbach, J. Phys. Chem. C **127**, 1891 (2023).

[47] Y. Cho, S. M. Greene, and T. C. Berkelbach, Phys. Rev. Lett. **126**, 216402 (2021).

[48] D. Weinberg, Y. Park, D. T. Limmer, and E. Rabani, Nano Lett. **23**, 4997 (2023).

[49] M. Parrinello and A. Rahman, J. Chem. Phys. **80**, 860 (1984).

[50] C. G. Bischak, M. Lai, Z. Fan, D. Lu, P. David, D. Dong, H. Chen, A. S. Etman, T. Lei, J. Sun *et al.*, Matter **3**, 534 (2020).

[51] M. Gao, Y. Park, J. Jin, P.-C. Chen, H. Devyldere, Y. Yang, C. Song, Z. Lin, Q. Zhao, M. Siron *et al.*, J. Am. Chem. Soc. **145**, 4800 (2023).

[52] L. N. Quan, Y. Park, P. Guo, M. Gao, J. Jin, J. Huang, J. K. Copper, A. Schwartzberg, R. Schaller, D. T. Limmer *et al.*, Proc. Natl. Acad. Sci. USA **118**, e2104425118 (2021).

[53] M. Sajedi, M. Krivenkov, D. Marchenko, J. Sánchez-Barriga, A. K. Chandran, A. Varykhalov, E. D. L. Rienks, I. Aguilera, S. Blügel, and O. Rader, Phys. Rev. Lett. **128**, 176405 (2022).

[54] K. Miyata, D. Meggiolaro, M. T. Trinh, P. P. Joshi, E. Mosconi, S. C. Jones, F. D. Angelis, and X.-Y. Zhu, Sci. Adv. **3**, e1701217 (2017).

[55] D. M. Ceperley, Rev. Mod. Phys. **67**, 279 (1995).

[56] See Supplemental Material at http://link.aps.org/supplemental/10.1103/PhysRevMaterials.7.106002 for additional details on the atomistic force field, pseudopotentials, wall potentials, the discretized Hamiltonian, and a thermodynamic perturbative theory approach used to extract the binding energies with dynamic approximation. It also contains Refs. [71–74].

[57] J. Schnitker and P. J. Rossky, J. Chem. Phys. **86**, 3462 (1987).

[58] R. A. Kuharski, J. S. Bader, D. Chandler, M. Sprik, M. L. Klein, and R. W. Impey, J. Chem. Phys. **89**, 3248 (1988).

[59] L.-W. Wang and A. Zunger, Phys. Rev. Lett. **73**, 1039 (1994).

[60] R. P. Feynman, *Statistical Mechanics* (CRC Press, Boca Raton, 1998).
[61] R. P. Feynman and A. R. Hibbs, *Quantum Mechanics and Path Integrals*, emended by D. F. Styer (Dover, Mineola, 2005).
[62] S. Habershon, D. E. Manolopoulos, T. E. Markland, and T. F. Miller III, Annu. Rev. Phys. Chem. **64**, 387 (2013).
[63] S. Plimpton, J. Comput. Phys. **117**, 1 (1995).
[64] D. Scharf, J. Jortner, and U. Landman, Chem. Phys. Lett. **130**, 504 (1986).
[65] M. F. Herman, E. J. Bruskin, and B. J. Berne, J. Chem. Phys. **76**, 5150 (1982).
[66] M. C. Brennan, A. Forde, M. Zhukovskyi, A. J. Baublis, Y. V. Morozov, S. Zhang, Z. Zhang, D. S. Kilin, and M. Kuno, J. Phys. Chem. Lett. **11**, 4937 (2020).
[67] S. T. Park, G. S. Jeen, H. Y. Kim, and I. G. Kim, J. Korean Phys. Soc. **37**, 309 (2000).
[68] Y. Z. Hu, S. W. Koch, M. Lindberg, N. Peyghambarian, E. L. Pollock, and F. F. Abraham, Phys. Rev. Lett. **64**, 1805 (1990).
[69] Y. Guo, O. Yaffe, T. D. Hull, J. S. Owen, D. R. Reichman, and L. E. Brus, Nat. Commun. **10**, 1175 (2019).
[70] M. C. Brennan, J. E. Herr, T. S. Nguyen-Beck, J. Zinna, S. Draguta, S. Rouvimov, J. Parkhill, and M. Kuno, J. Am. Chem. Soc. **139**, 12201 (2017).
[71] Q. Zhao, A. Hazarika, L. T. Schelhas, J. Liu, E. A. Gaulding, G. Li, M. Zhang, M. F. Toney, P. C. Sercel, and J. M. Luther, ACS Energy Lett. **5**, 238 (2020).
[72] R. X. Yang, J. M. Skelton, E. L. da Silva, J. M. Frost, and A. Walsh, J. Phys. Chem. Lett. **8**, 4720 (2017).
[73] Y. Han, W. Liang, X. Lin, Y. Li, F. Sun, F. Zhang, P. C. Sercel, and K. Wu, Nat. Mater. **21**, 1282 (2022).
[74] T. Sometani, Eur. J. Phys. **21**, 549 (2000).